Supplementary Information for

# Submesoscales are a significant turbulence source in global ocean surface boundary layer

Jihai Dong*, Baylor Fox-Kemper, Jacob O. Wenegrat, Abigail S. Bodner, Xiaolong Yu, Stephen Belcher, Changming Dong*

*Corresponding authors: Changming Dong, cmdong@nuist.edu.cn; Jihai Dong, jihai_dong@nuist.edu.cn

The supplementary information includes:

- Supplementary Figures 1-13
- Supplementary Table 1

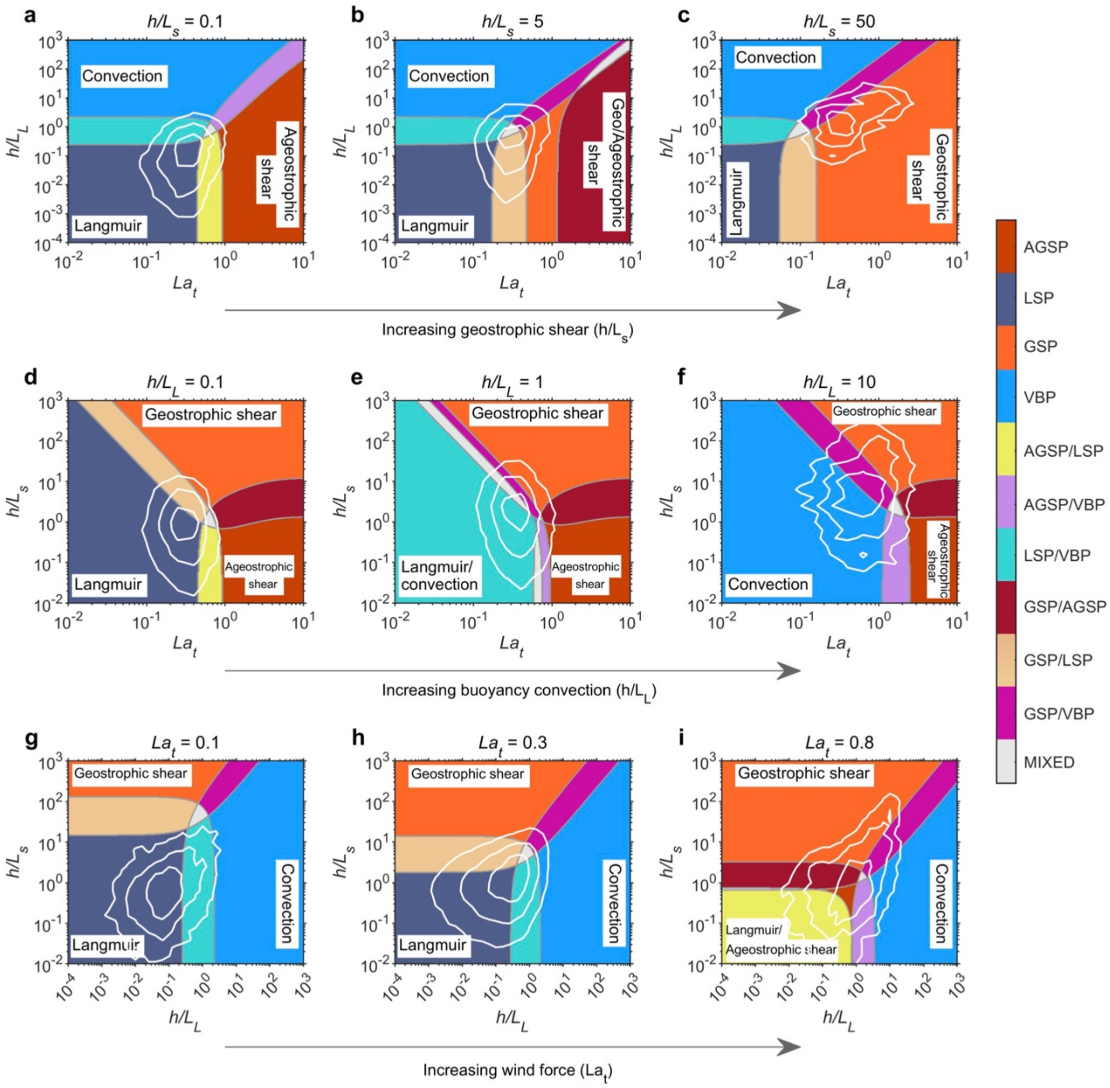


**Supplementary Fig. 1 Turbulence regimes in different parameter slices in summer.** The regimes (GSP: geostrophic shear production turbulence; LSP: Langmuir shear production turbulence; VBP: vertical buoyancy production turbulence; AGSP: ageostrophic shear production turbulence) denoted by different color patches are defined by the dominant production terms in the TKE budget in different parameter slices. The white contours enclose 30%, 60%, and 90% of the locations with the corresponding values. A regime is considered dominant when its dissipation contribution exceeds 75% of the total dissipation, otherwise, it is a two-turbulence-mixed regime when two TKE sources both contribute more than 25% while all others contribute less than 25%, and lastly, it is a mixed regime if more than three kinds of turbulence contribute more than 25% (Li et al., 2019). Compared with **Fig. 2**, the magnitude of GSP is much weakened in summer.

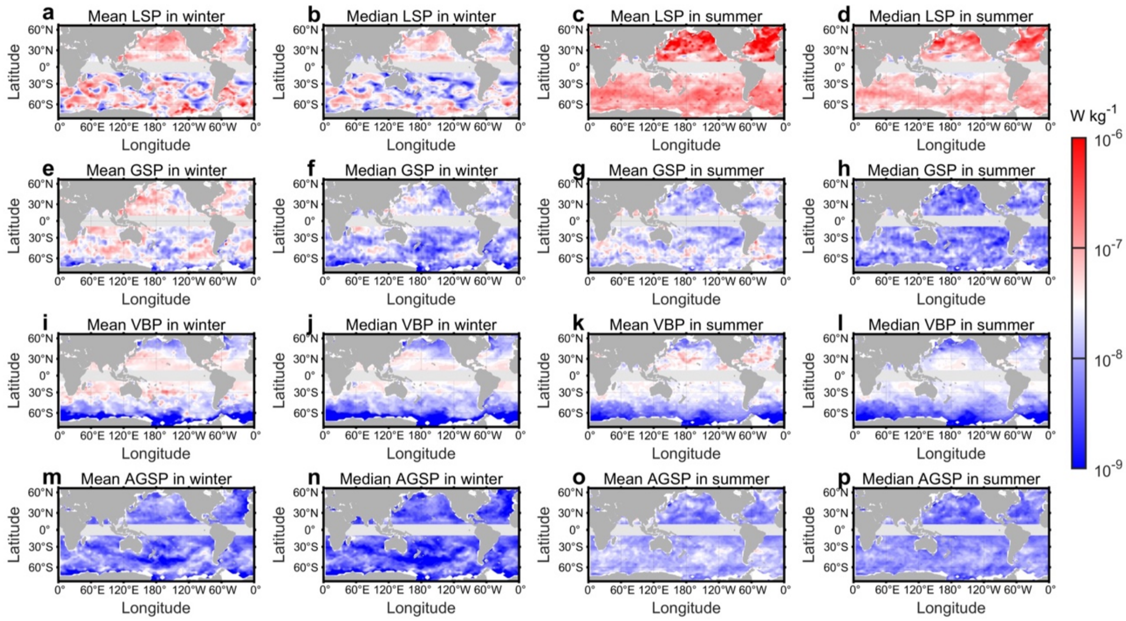


**Supplementary Fig. 2. Global distributions of the dissipation rates. a**-**d**, Langmuir shear production turbulence (LSP). **e**-**h**, geostrophic shear production turbulence (GSP). **i**-**l,** vertical buoyancy production turbulence (VBP). **m**-**p**, ageostrophic shear production turbulence (AGSP). The dissipation rates are derived from the TKE model based on the LLC4320 data. The columns from left to right show the means in winter, the medians in winter, the means in summer and the medians in summer, respectively. Both means and medians suggest the importance of GSP turbulence over the globe.

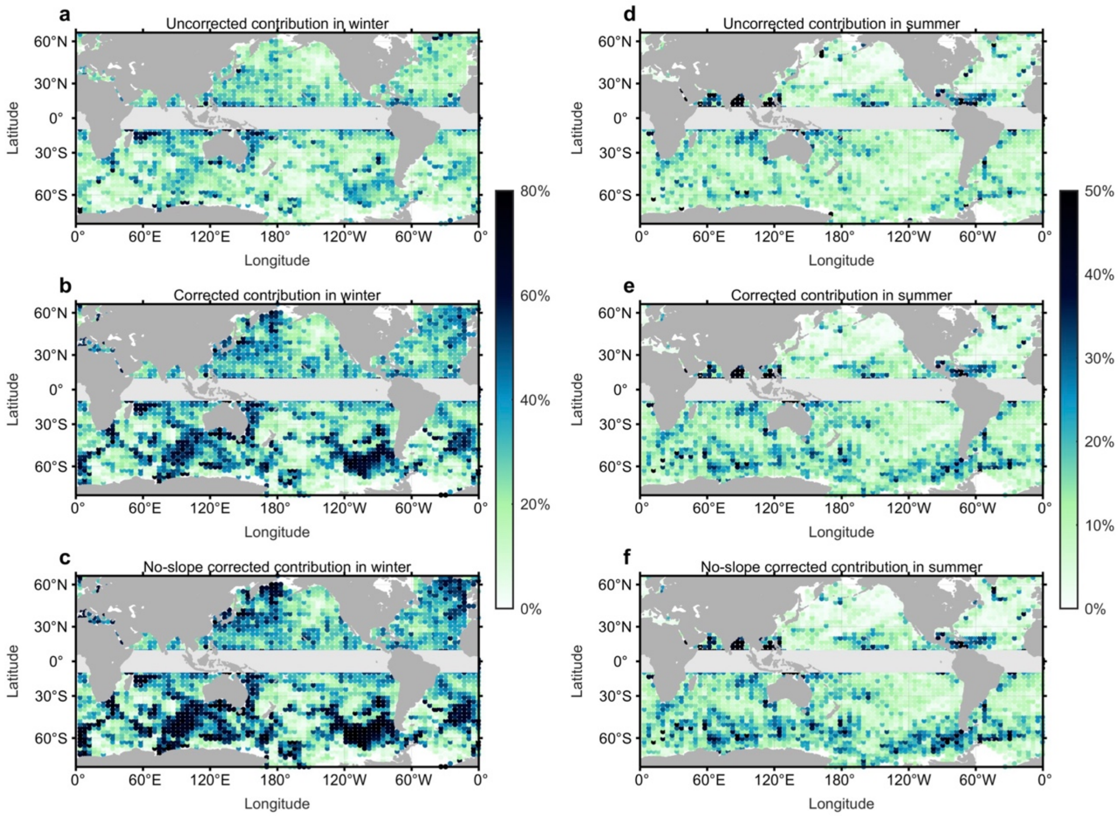


**Supplementary Fig. 3 The relative contribution percentages of geostrophic shear production turbulence (GSP) to the dissipation rate in the surface boundary layer. a, d,** The results based on uncorrected buoyancy gradients. **b**, **e**, The results based on corrected buoyancy gradients. **c**, **f**, The results based on no-slope corrected buoyancy gradients (left: winter; right: summer). The relative contribution of GSP explicitly shows where GSP dominates the boundary layer turbulence, and also suggests a robust role of GSP turbulence due to the buoyancy gradient correction.

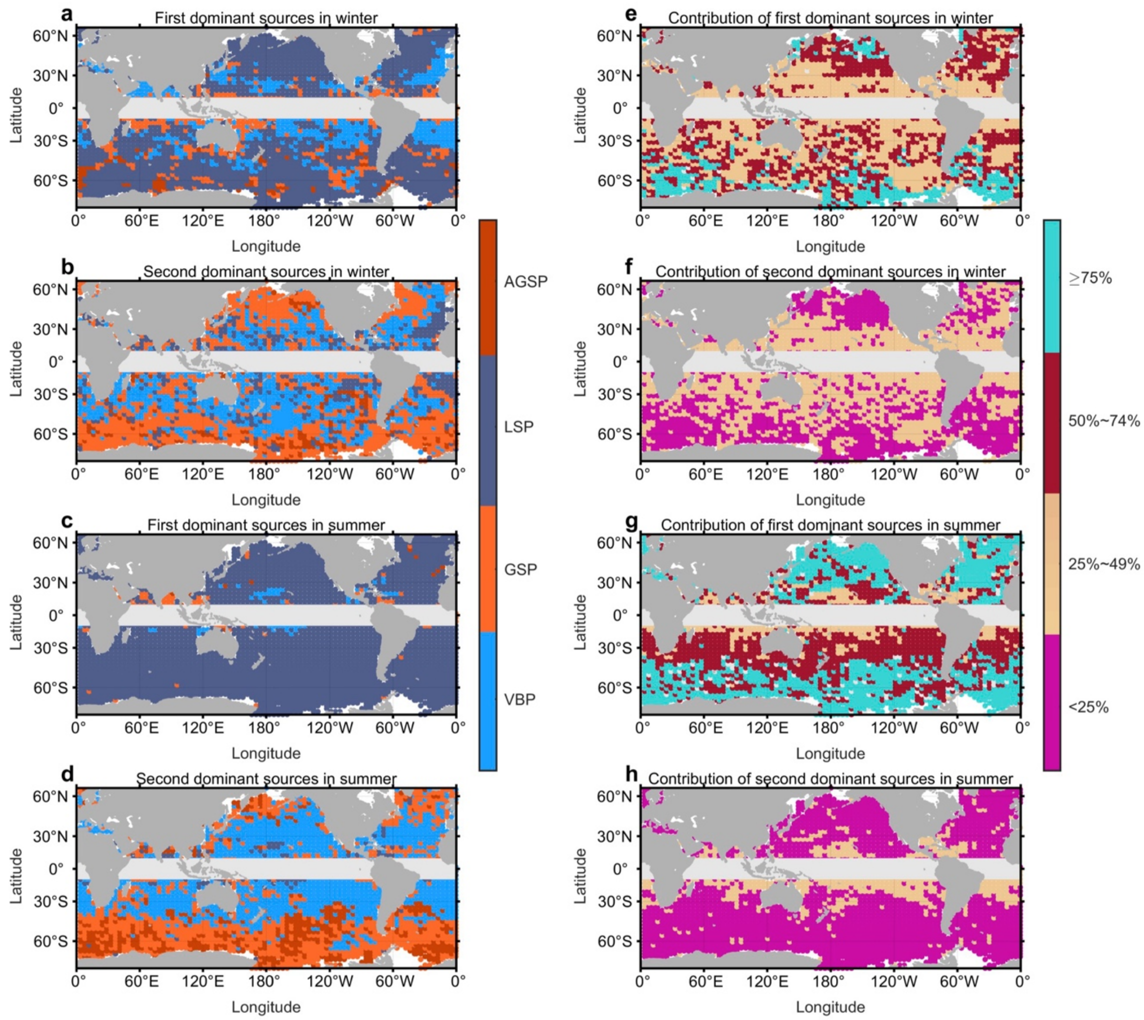


**Supplementary Fig. 4 Global distributions of the two most likely dominant sources at each location.** The results are based on the uncorrected buoyancy gradients. **a**, The first most likely dominant sources (GSP: geostrophic shear production turbulence; LSP: Langmuir shear production turbulence; VBP: vertical buoyancy production turbulence; AGSP: ageostrophic shear production turbulence) in winter. **b**, The second most likely dominant sources in winter. **c**, The first most likely dominant sources in summer. **d**, The second most likely dominant sources in summer. Their relative contribution percentages to the total mean dissipation (%) are shown in **e**-**h**. Despite that GSP turbulence is weakened, it is still a significant contributor at low latitudes in winter, and the second largest contributor at high latitudes in both seasons. S

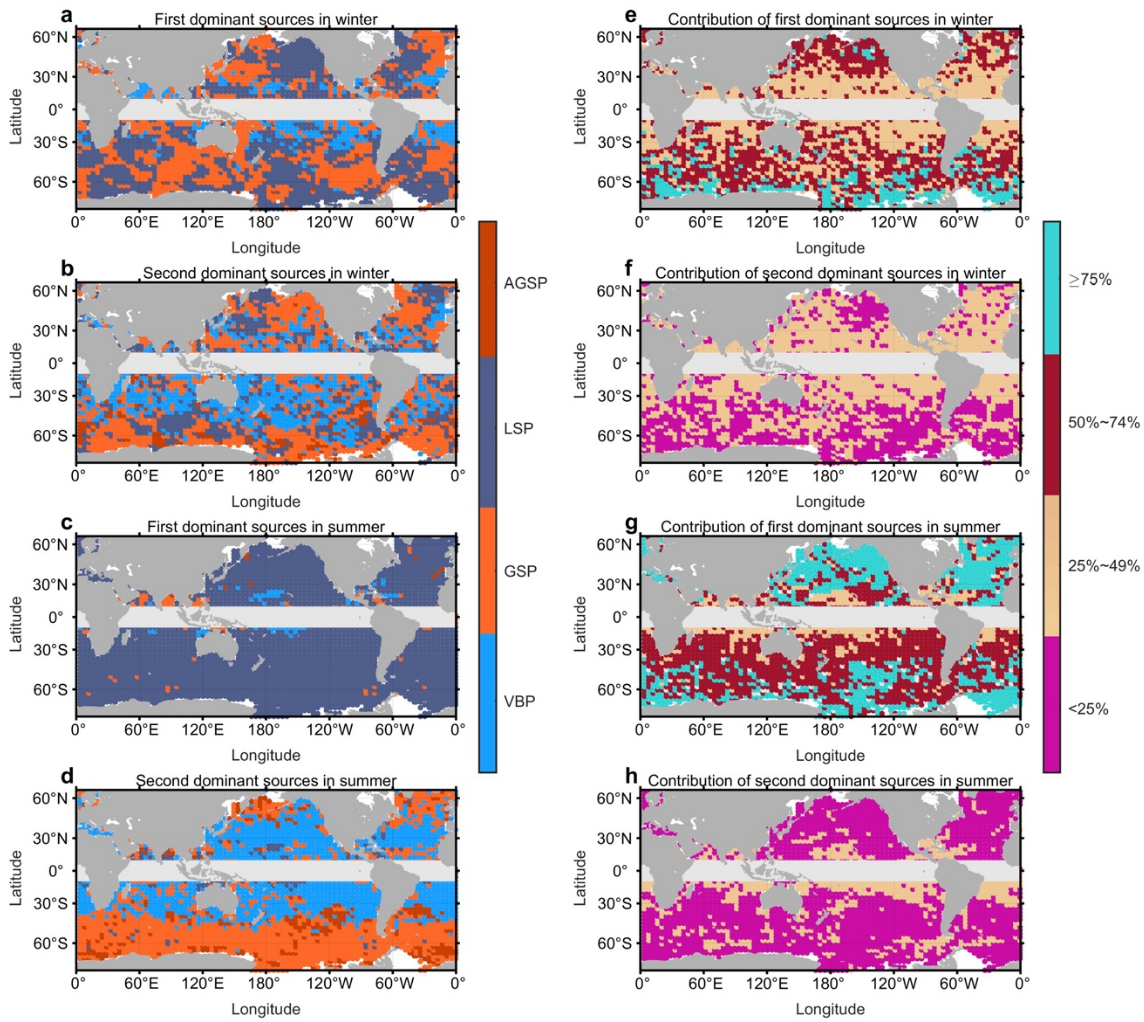


**Supplementary Fig. 5 Global distributions of the two most likely dominant sources at each location**. The results are based on the no-slope corrected buoyancy gradients. **a,** The first most likely dominant sources (GSP: geostrophic shear production turbulence; LSP: Langmuir shear production turbulence; VBP: vertical buoyancy production turbulence; AGSP: ageostrophic shear production turbulence) in winter. **b,** The second most likely dominant sources in winter. **c,** The first most likely dominant sources in summer. **d,** The second most likely dominant sources in summer. Their relative contribution percentages to the total mean dissipation (%) are shown in **e-h.** As GSP turbulence is strengthened, it becomes the most prevalent contributor of the first-dominant sources in winter.

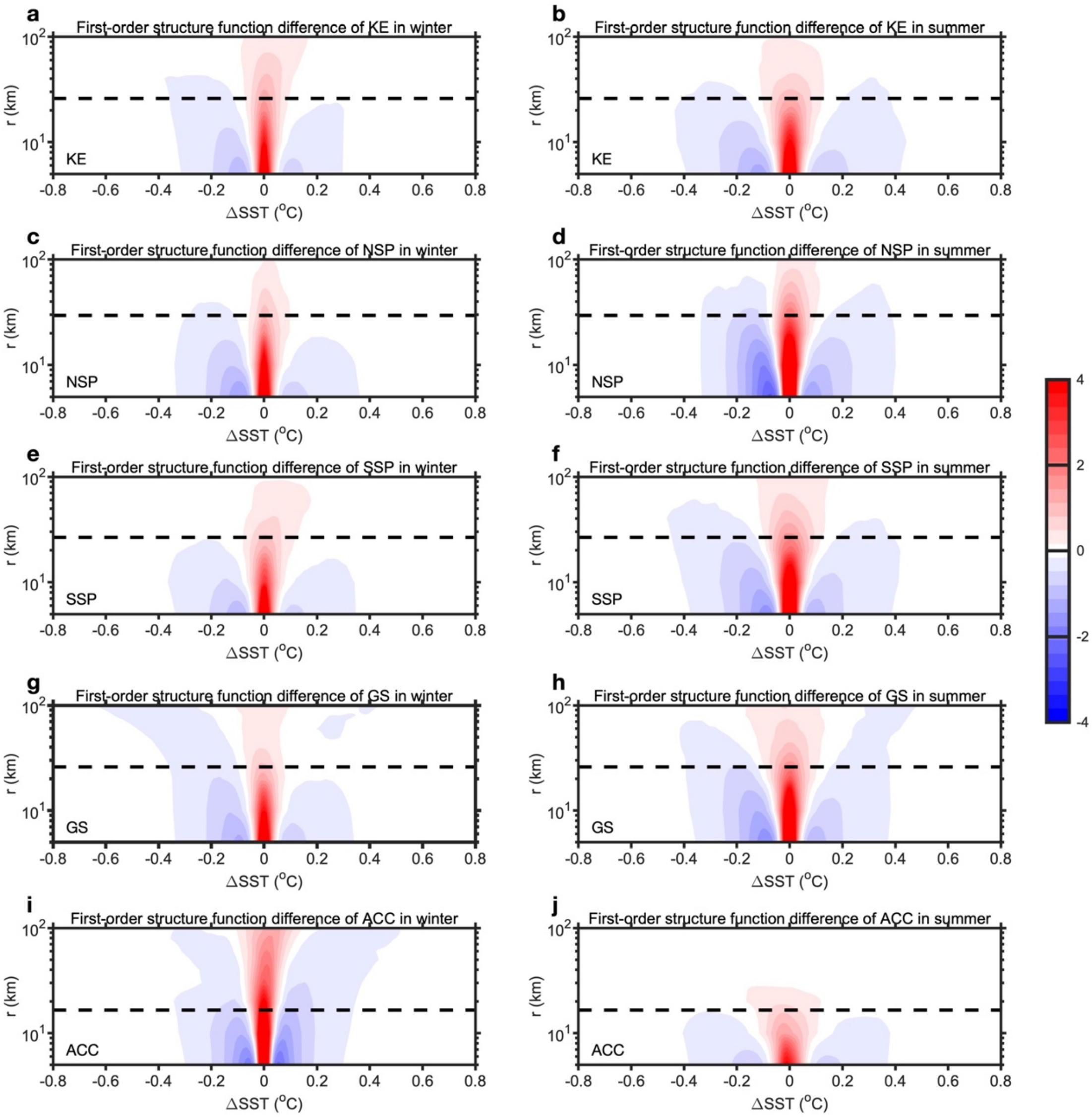


**Supplementary Fig. 6 Probability density function differences of the first-order structure functions of sea surface temperature (SST) in different regions. a, b,** the Kuroshio Extension (KE; 32~38 $^{o}$N, 150~156 $^{o}$E). **c, d,** the Northern Subtropical Pacific (NSP; 15~21 $^{o}$N, 180~186 $^{o}$E). **e, f,** the Southern Subtropical Pacific (SSP; 20~26 $^{o}$S, 120~126 $^{o}$W). **g, h,** the Gulf Stream (GS; 28~34 $^{o}$N, 60~66 $^{o}$W). **i, j,** the Antarctic Circumpolar Current (ACC; 50~56 $^{o}$S, 115~121 $^{o}$E) (left: winter; right: summer). The dashed lines denote the minimum wavelengths that the effective resolution resolves (i.e., two times the effect resolution 7Δx). The positive bias in probability at small SST jump magnitude and negative bias in probability at large SST jump magnitude imply that at small spatial scale LLC4320 underpredicts large SST jumps compared to the real ocean, which needs to be corrected.

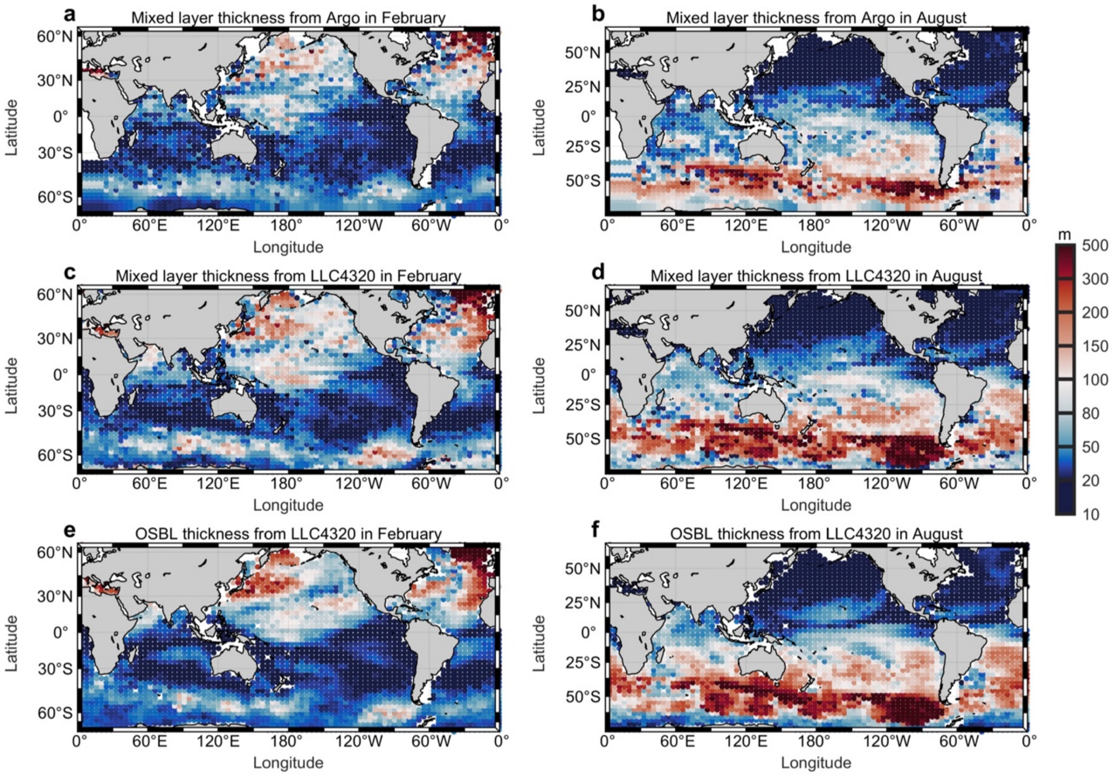


**Supplementary Fig. 7 Comparison of the ocean surface boundary layer (OSBL) and sea surface mixed layer thicknesses in different seasons (m). a, b, c,** the thicknesses in February 2012**. d, e, f,** the thicknesses in August 2012**.** The upper, middle, and lower panels show the mixed layer thickness from Argo, LLC4320, and the OSBL thickness from LLC4320, respectively. The mixed layer depth is defined as the depth where a temperature variance of 0.2ºC occurs compared to the 10-m depth temperature. The similarity of the global pattern demonstrates the capability of LLC4320 to reproduce the ocean surface layer.

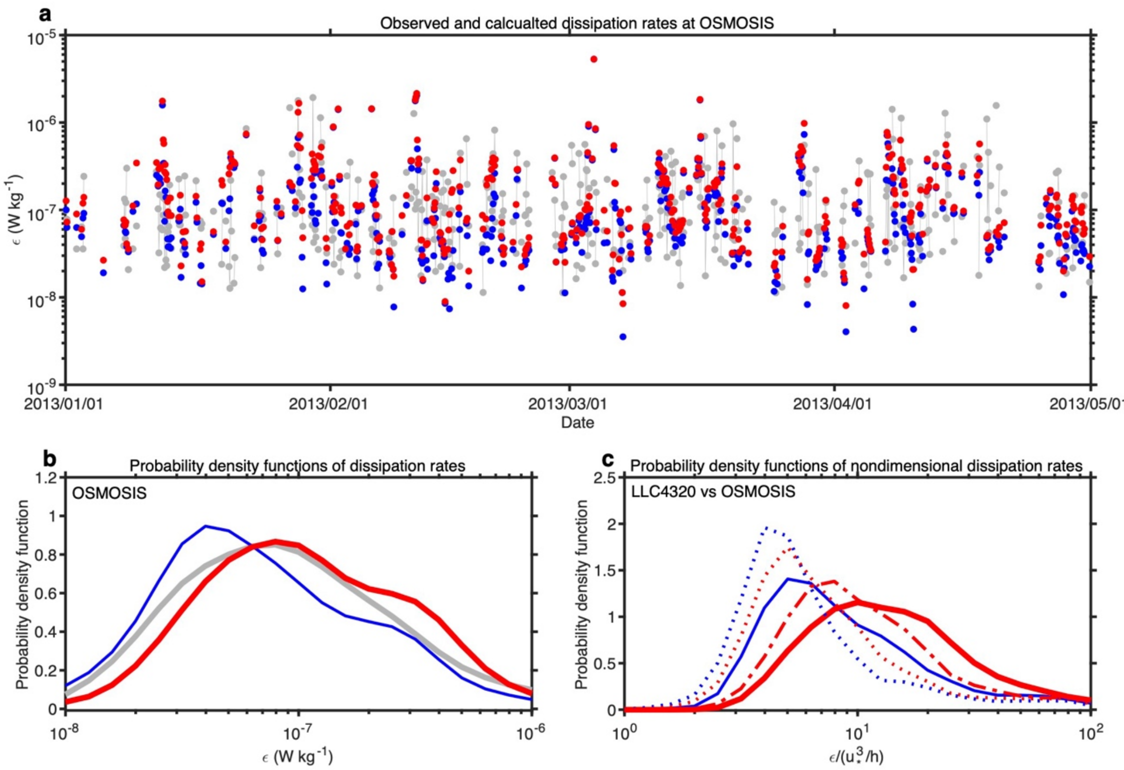


**Supplementary Fig. 8 Dissipation rates at OSMOSIS and its comparison to LLC4320. a**, Time series of the dissipation rates at the boundary layer mid-depth of the OSMOSIS site over the winter time (January 2013–April 2013). **b**, probability density functions of the dissipation rates. The gray dots and lines denote the observed values, while the blue and red ones denote the calculated values (the blues are the summation of dissipation from Langmuir shear production turbulence (LSP), vertical buoyancy production turbulence (VBP) and ageostrophic shear production turbulence (AGSP), while the reds are from geostrophic shear production turbulence (GSP), LSP, VBP and AGSP). A comparison of the non-dimensional dissipation magnitudes between observations (solid lines) and LLC4320 (dotted and dotted-dash lines; the same winter time but in 2012) is shown in **c** (dash blue: observed LSP+VBP+AGSP; solid blue: observed LSP+ corrected GSP+VBP+AGSP; dash red: simulated LSP+GSP+VBP+AGSP; dotted line: simulated LSP+ uncorrected GSP+VBP+AGSP; dotted dash line: simulated LSP+ corrected GSP+VBP+AGSP).

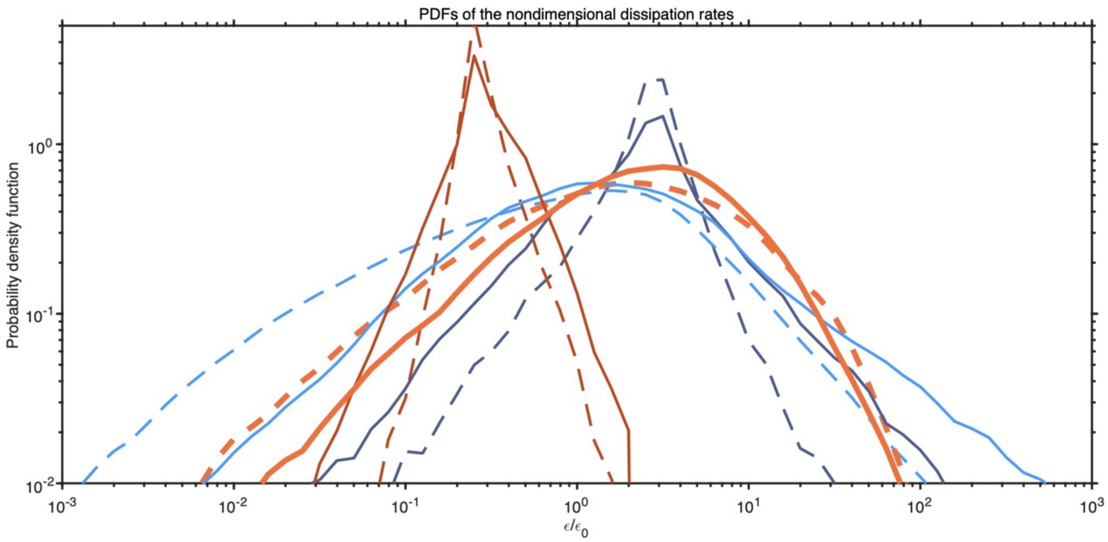


**Supplementary Fig. 9 Probability density functions (PDFs) of the nondimensional dissipation rates of turbulence sources from different simulations. The four sources are** geostrophic shear production turbulence (GSP; orange), Langmuir shear production turbulence (LSP; dark blue;), vertical buoyancy production turbulence (VBP; light blue), and ageostrophic shear production turbulence (AGSP dark red)The dash and solid lines show the results from LLC4320 and eNATL60, respectively. The similarity of the PDF distributions demonstrates the robust role of GSP turbulence.

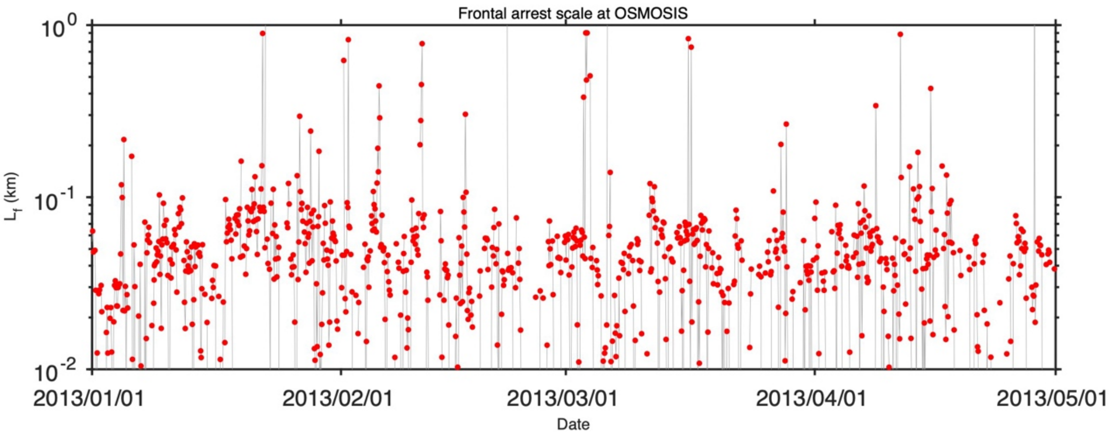


**Supplementary Fig. 10 The frontal arrest scale.** The estimated frontal arrested scale under the turbulent thermal-wind balance at the OSMOSIS site based on the method of Bodner et al. (2023). The frontal scale cannot be resolved by the OSMOSIS mooring array.

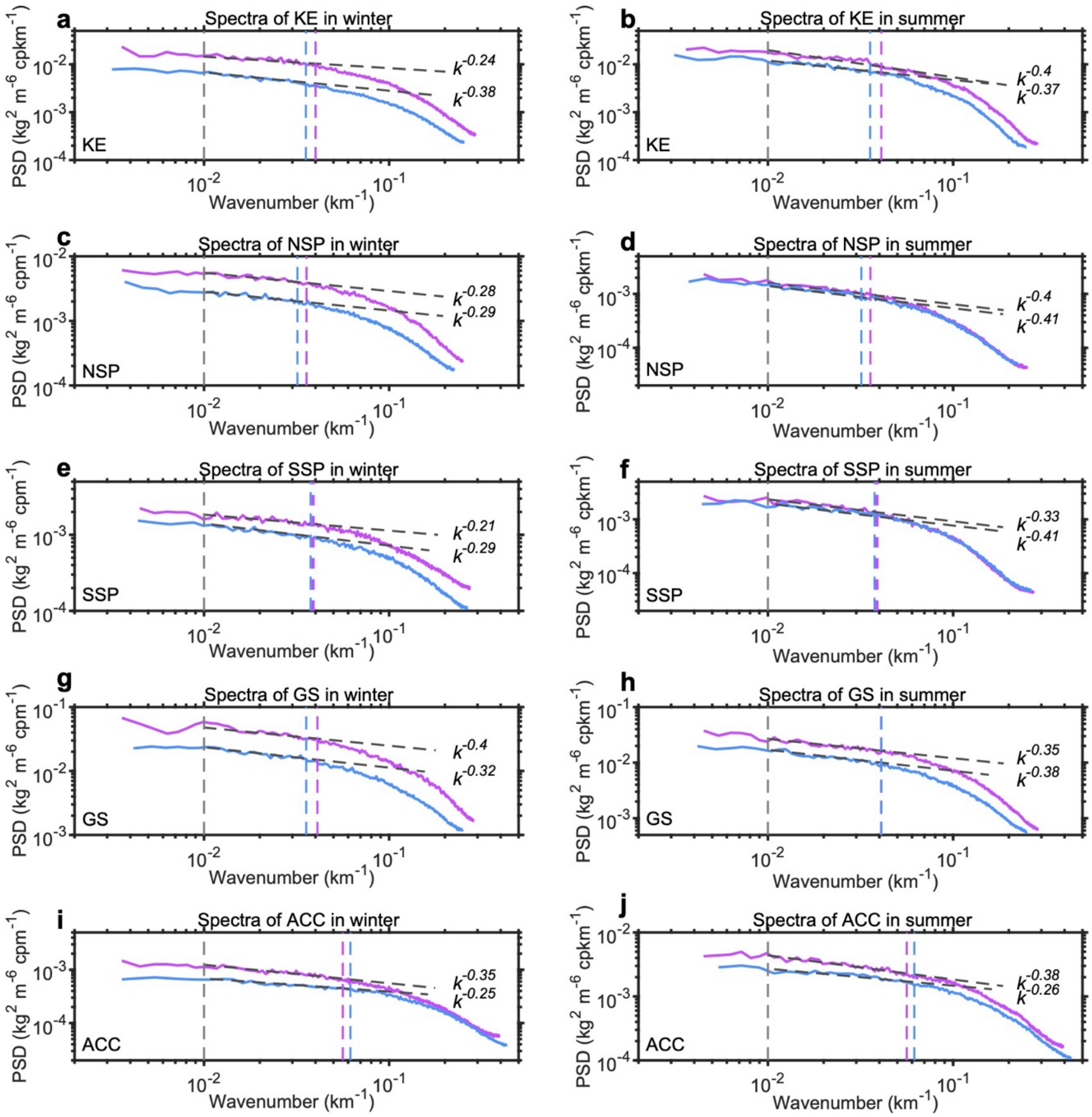


**Supplementary Fig. 11 Spectral slopes of the horizontal buoyancy gradient in different regions.** **a**, **b,** the Kuroshio Extension (KE; 32~38°N, 150~156 °E). **c**, **d,** the Northern Subtropical Pacific (NSP; 15~21 °N, 180~186 °E). **e**, **f,** the Southern Subtropical Pacific (SSP; 20~26 °S, 120~126 °W). **g**, **h,** the Gulf Stream (GS; 28~34 °N, 60~66 °W). **i**, **j,** the Antarctic Circumpolar Current (ACC; 50~56 °S, 115~121 °E) (left: winter; right: summer). The blue and pinks lines denote the power spectral densities of the horizontal buoyancy gradient in zonal and in meridional, respectively. The dashed gray lines denote the corresponding linearly fitted slopes of the inertial range. The vertical dash lines denote the maximum wavenumber that the effective resolution resolves (i.e., two times the effective resolution 7Δx). The spectral slopes from LLC4320 generally have slightly negative slopes, rather than zero slopes.

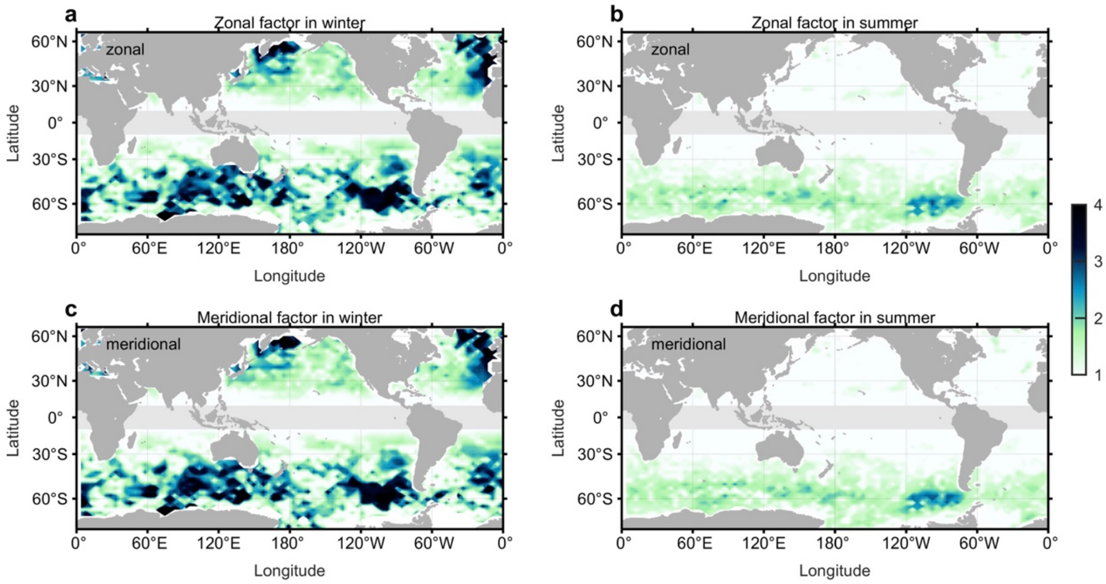


**Supplementary Fig. 12 Global distributions of the amplification factors**. **a**, **b,** the amplification factor of the zonal buoyancy gradient. **c**, **d,** the amplification factor of the meridional buoyancy gradient (left: winter; right: summer). This amplification is because the spatial resolution of LLC4320 cannot resolve the arrested fronts under the turbulent thermal-wind balance.

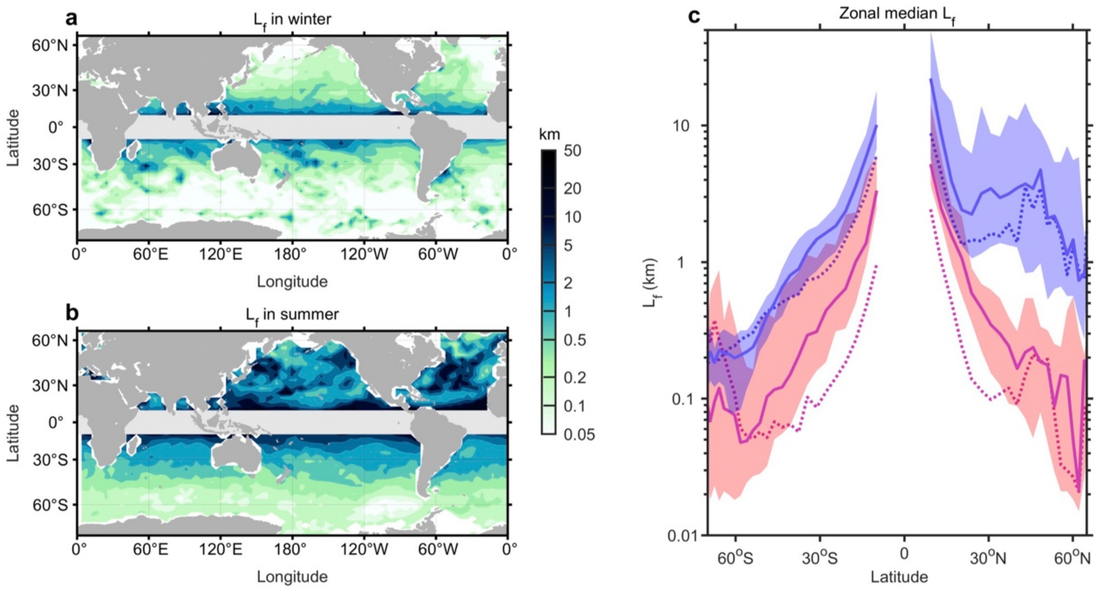


**Supplementary Fig. 13 Global distributions of the frontal scale $L_f$ (km). a,** $L_f$ in winter. **b,** $L_f$ in summer. **c,** the zonal median $L_f$ (winter in pink and summer in blue). The solid and dashed lines in **c** denote the values derived from the LCC4320 and GOTM results and the shaded intervals denote the corresponding bounds of the 10th and 90th percentile $L_f$ values of the LLC4320 zonally. The frontal arrested scale is latitude-dependent and insensitive to the turbulence closures.

**Supplementary Table 1 Percentages of locations and contributions.** Percentages of locations globally where each energy source is either the first or second largest contribution and their global averages $\boldsymbol{\varepsilon_{avg}}$ and 10th and 90th percentiles, $\boldsymbol{\varepsilon_{10th}}$, $\boldsymbol{\varepsilon_{90th}}$ of the dissipation rate (×$10^{-8}$ W $kg^{-1}$), by season. The differences in results due to different levels of correction for limited horizontal model resolution are shown. GSP: geostrophic shear production turbulence; LSP: Langmuir shear production turbulence; VBP: vertical buoyancy production turbulence; AGSP: ageostrophic shear production turbulence.

| Method | | Source: LSP win | LSP sum | GSP win | GSP sum | VBP win | VBP sum | AGSP win | AGSP sum |
|---|---|---|---|---|---|---|---|---|---|
| Uncorrected | 1st, 2nd | 52%, 24% | 84%, 10% | 25%, 32% | 11%, 27% | 22%, 39% | 5%, 53% | 1%, 5% | 0%, 10% |
| | $\varepsilon_{avg}$ [$\varepsilon_{10th}$, $\varepsilon_{90th}$] | 9.6 [0.38, 13] | 25 [1.2, 34] | 3.0 [0.087, 8.1] | 2.4 [0.075, 6.9] | 4.9 [0.082, 5.8] | 3.6 [0.13, 4.9] | 0.87 [0.041, 2.0] | 1.4 [0.14, 2.9] |
| Corrected | 1st, 2nd | 44%, 26% | 84%, 10% | 37%, 34% | 11%, 31% | 16%, 35% | 4%, 52% | 3%, 4% | 1%, 7% |
| | $\varepsilon_{avg}$ [$\varepsilon_{10th}$, $\varepsilon_{90th}$] | same as above | same as above | 4.6 [0.11, 12] | 2.6 [0.087, 7.7] | same as above | same as above | same as above | same as above |
| No-slope corrected | 1st, 2nd | 41%, 28% | 84%, 10% | 45%, 35% | 11%, 32% | 14%, 35% | 4%, 52% | 0%, 2% | 1%, 6% |
| | $\varepsilon_{avg}$ [$\varepsilon_{10th}$, $\varepsilon_{90th}$] | same as above | same as above | 5.6 [0.13, 15] | 2.7 [0.093, 8.3] | same as above | same as above | same as above | same as above |

## Supplementary References

1. Li Q, Reichl BG, Fox-Kemper B, Adcroft AJ, Belcher SE, Danabasoglu G*, et al.* Comparing ocean surface boundary vertical mixing schemes including Langmuir turbulence. *Journal of Advances in Modeling Earth Systems* 2019, **11**(11)**:** 3545-3592

2. Bodner AS, Fox-Kemper B, Johnson L, Van Roekel LP, McWilliams JC, Sullivan PP*, et al.* Modifying the Mixed Layer Eddy Parameterization to Include Frontogenesis Arrest by Boundary Layer Turbulence. *Journal of Physical Oceanography* 2022, **53**(1), 323-339